

Testing helicity dependent $\gamma\gamma \rightarrow \gamma\gamma$ scattering in the region of MeV

K. Homma,^{1,2} K. Matsuura,¹ and K. Nakajima³

¹*Graduate School of Science, Hiroshima University,*

Kagamiyama, Higashi-Hiroshima 739-8526, Japan

²*International Center for Zetta-Exawatt Science and Technology,
Ecole Polytechnique, Route de Saclay, Palaiseau, F-91128, France*

³*Center for Relativistic Laser Science, Institute for Basic
Science (IBS), Gwangju 500-712, Republic of Korea*

(Dated: June 13, 2021)

Abstract

Light-by-light scatterings contain rich information on the photon coupling to virtual and real particle states. In the context of quantum electrodynamics (QED), photons can couple to a virtual e^+e^- pair. Photons may also couple to known resonance states in the context of quantum chromodynamics and electroweak dynamics in higher energy domains and possibly couple to unknown resonance states beyond the standard model. The perturbative QED calculations manifestly predict the maximized cross section at the MeV scale, however, any example of the exact real-photon - real-photon scattering has not been observed hitherto. Hence, we propose the direct measurement with the maximized cross-section at the center-of-mass system energy of 1-2 MeV to establish the firm footing at the MeV scale. Given currently state-of-the-art high power lasers, the helicity dependent elastic scattering may be observed at a reasonable rate, if a photon-photon collider exploiting γ -rays generated by the inverse nonlinear Compton process with electrons delivered from laser-plasma accelerators (LPA) are properly designed. We show that such verification is feasible in a table-top scale collider which may be an unprecedented breakthrough in particle accelerators for basic physics research in contrast to energy frontier colliders.

PACS numbers: 12.20.-m,12.20.Fv,14.80.Va,29.20.db,41.75.Jv,42.62.-b

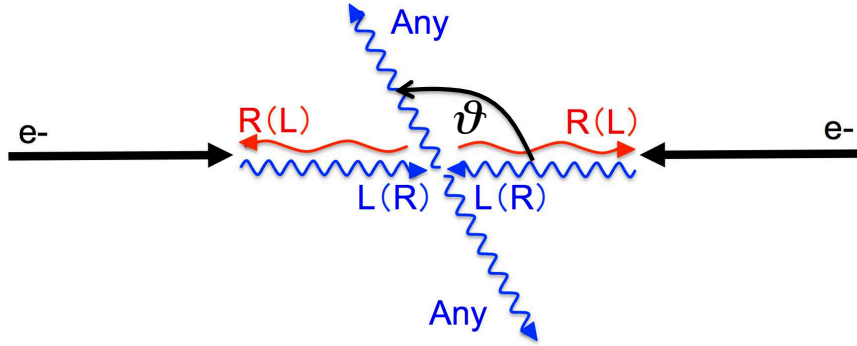


FIG. 1: Helicity configuration in $\gamma\gamma$ scattering via inverse Compton scatterings between circularly polarized laser pulses and unpolarized electrons. R and L denote right- and left-handed helicity states of photons, respectively.

I. INTRODUCTION

Light-by-light scattering is a purely quantum process, hence, in the standard model, only possible in the context of quantum electrodynamics (QED). QED is the most strictly tested dynamics in its perturbative regime. The scattering amplitude in the lowest order is described by the box diagram where a virtual e^+e^- pair loops between four external photons. So far the diagram is indirectly confirmed with off-shell external photons via $\gamma A \rightarrow \gamma A$ [1] known as Delbrück scattering [2] and also proposed to be further tested via $AA \rightarrow AA\gamma\gamma$ in the higher energy domain at the Large Hadron Collider [3]. In these scatterings, however, photons are emitted from nuclei A and have finite off-shell masses. With the exact on-shell condition, namely, real-photon - real-photon scattering has not been demonstrated hitherto despite of its explicit predictions [4–8]. Moreover, its dependence on the photon polarization states has not been tested at all. By means of off-shell incident photons from nuclei, it is difficult to test the polarization property. Photon-photon interactions also contain rich information on the two-photon coupling to standard model / non-standard model resonance states depending on the center of mass energy. In the MeV range, no direct search for resonance states coupling to two photons has been performed. Therefore, it is indispensable to first verify the purely QED-based scattering amplitude with specified polarization states in a pristine experimental condition, because a significant deviation from the prediction indicates the existence of physics beyond the standard model.

In lower energies, searches for photon-photon interactions have been performed at keV [9],

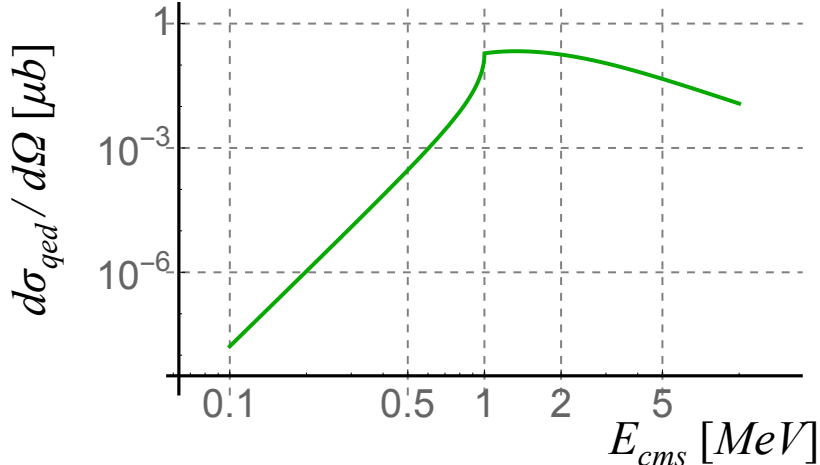


FIG. 2: The unpolarized QED-based differential cross section $d\sigma_{qed}/d\Omega$ at $\vartheta = \pi/2$ in units of μb as a function of the center-of-mass system energy in photon-photon collisions, E_{cms} .

eV [10, 11] and sub-eV energy scales attempting to search for dark matter [12–20] and also to put the upper limit on the QED photon-photon interaction [21]. There are several proposals [22–25] to probe photon-photon interactions in the context of the low energy limit of the QED interactions [26, 27] based on only optical photons. These proposals commonly suffer from its extremely weak interaction. Therefore, currently state-of-the-art high-power lasers are supposed to be indispensable. However, if such lasers are available, we may also use them to generate γ -rays. This idea leads us to try to consider the direct measurement of the scattering with the maximized cross-section at the center-of-mass system energy of 1-2 MeV rather than based on 1 eV photons.

In this paper we discuss the feasibility to measure the helicity dependent $\gamma\gamma$ -scattering based on the helicity configuration as illustrated in Fig.1 where circularly polarized laser pulses are reflected upon unpolarized electron bunches and γ -rays in the same helicity state collide head-on. We then consider to measure the elastic scattering without specifying the helicity states of the final state γ -rays. In contrast to the helicity dependence emphasizing on the forward scattering amplitude [28, 29], we rather aim at larger angle scattering events in order to verify the purely perturbative prediction. In the following paragraphs, we discuss the QED-based helicity dependent $\gamma\gamma$ -scattering cross section, how to produce electrons with LPA, the expected helicity specified γ -ray yield based on the nonlinear Compton process and then possibility to realize a realistic experiment.

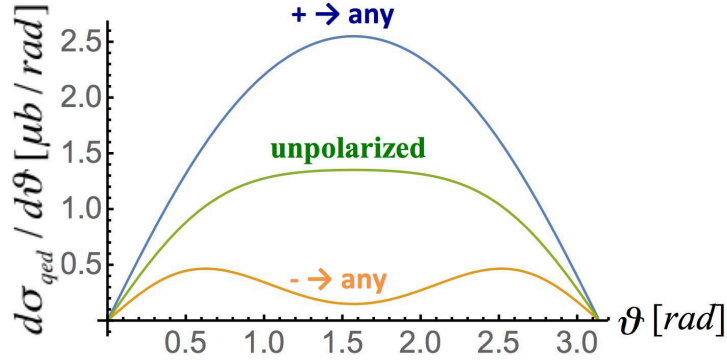


FIG. 3: Helicity dependence of QED-based differential cross sections at $E_{cms} = 1.4$ MeV as a function of the photon scattering angle ϑ in CMS.

II. QED-BASED PHOTON-PHOTON INTERACTION

The elastic scattering of photons by photons has been thoroughly evaluated in [6–8]. The differential cross section per solid angle for the unpolarized photon-photon scattering in the lower energy limit is approximated as $\frac{d\sigma_{qed}}{d\Omega} \sim \frac{\alpha^2 r_0^2}{4\pi^2} \frac{139}{(90)^2} \left(\frac{k}{m}\right)^6 (3 + \cos\vartheta)^2$, where m is electron mass in units of $\hbar = c = 1$, k is the incident photon energy in the center-of-mass system, $\alpha = 1/137$ is the dimensionless fine structure constant, $r_0 = \alpha/m \sim 2.8 \times 10^{-13}$ cm is the classical electron radius, and ϑ is the polar angle of scattered photons with respect to the colliding axis between two incident photons in the center-of-mass system on the reaction plane. For laser photons of $k \sim 1$ eV, the total cross section is $\sigma \sim 10^{-42}$ b. This is extremely small due to the steep k^6 dependence. This situation is shown in Fig.2 where the differential cross section of the unpolarized photon-photon elastic scattering, $d\sigma_{qed}/d\Omega$ at $\vartheta = \pi/2$, is plotted as a function of the center-of-mass system energy of photon-photon collisions, E_{cms} . The cross section curve is obtained from the numerical calculation applying formulae in Ref. [8]. On the other hand, if $k = 0.5 - 1.0$ MeV is realized, the total cross section is maximized up to $\sigma \sim 1 \mu\text{b}$. Therefore, in order to detect the perturbative QED cross section, it is reasonable to perform the scattering experiment tuned at that energy range. In the region $E_{cms} = 1 - 2$ MeV, we see a flat-top character. This allows relatively large fluctuations on E_{cms} , which is preferable for the photon-photon collider exploiting γ -rays via laser Compton scattering off electrons from LPA having a percent-level energy spread.

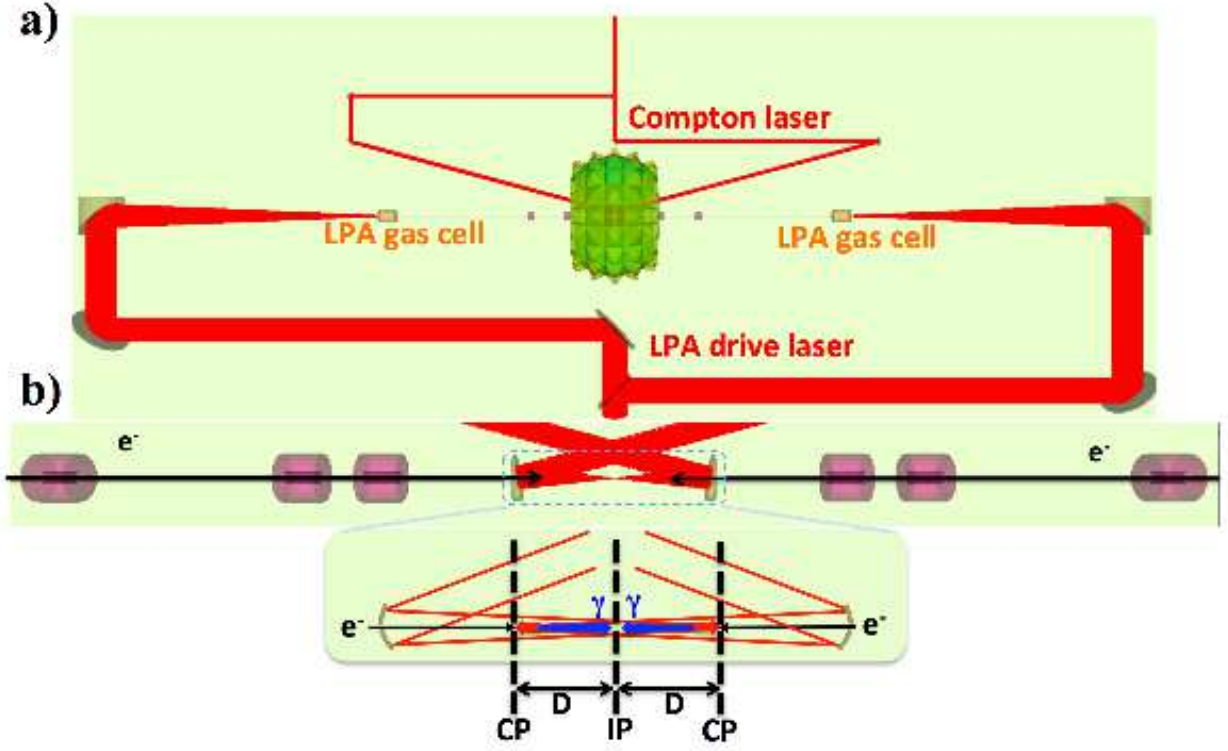


FIG. 4: An all-optical table-top ($3.4 \text{ m} \times 1.3 \text{ m}$) $\gamma\gamma$ -collider: a) top-view including two LPAs and the detector system to capture the $\gamma\gamma \rightarrow \gamma\gamma$ scattering and b) collision geometry around the interaction point, IP, where γ -rays are produced at each Compton scattering point (CP) in head-on collisions and D is the distance between IP and CP.

Figure 3 shows the helicity dependent QED-based differential cross section $d\sigma^{\pm \rightarrow \text{any}}/d\theta$ compared to the unpolarized cross section where the symbols $\pm \rightarrow \text{any}$ indicate the same and opposite helicity states between incident two γ -rays going to all the possible helicity states. These predictions are results of numerical calculations at $E_{cms} = 1.4 \text{ MeV}$ based on Ref. [8]. We find a larger cross section in the same helicity incidence case particularly around $\vartheta \sim \pi/2$.

III. TABLE-TOP $\gamma\gamma$ -COLLIDER

Figure 4 a) shows a table-top ($3.4 \text{ m} \times 1.3 \text{ m}$) $\gamma\gamma$ -collider with a realistic detector system to capture large angle $\gamma\gamma \rightarrow \gamma\gamma$ scattering events. The system consists of two LPAs to generate electron beams with which two incident γ -beams are further produced via the

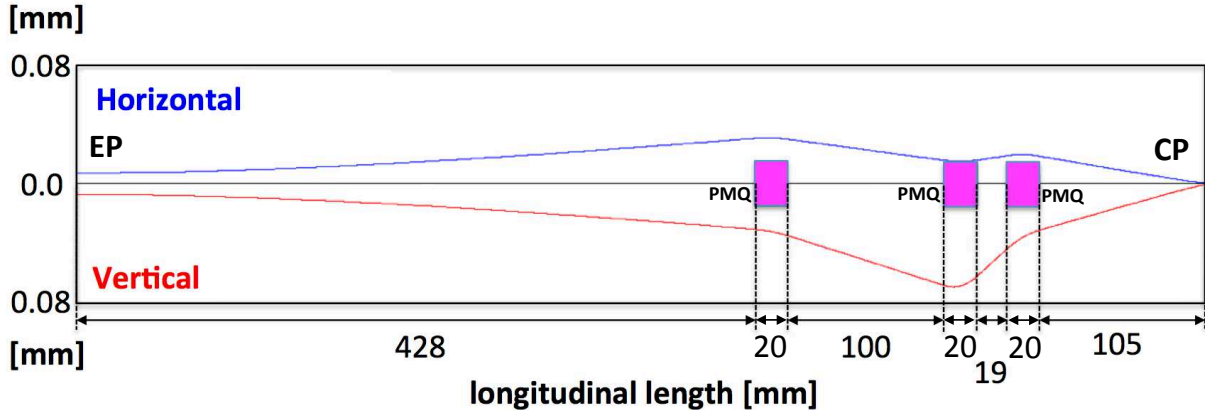


FIG. 5: A focusing system for an electron beam produced by LPA consisting of three PMQs from the ejection point (EP) of the electron beam at the gas cell for LPA to the inverse Compton scattering point (CP). The blue and red curves are traces of beam envelopes simulated by TRACE3D [37] for horizontal and vertical directions, respectively.

inverse Compton process in head-on collisions. Initially synchronized two laser pulses are incident from the top and bottom sides of the top view, respectively. They are individually split into two drive pulses for LPA and scatter pulses for the successive inverse Compton process with electrons delivered from LPA. Figure 4 b) illustrates the collision geometry around the interaction point (IP) of $\gamma\gamma$ -scattering, which is located at the distance D from the inverse Compton scattering point (CP).

An electron beam with 210 MeV and 1.6 nC are produced from a two-stage laser wakefield accelerator [30] comprising a 5-mm long gas cell filled with the mixed gas (e.g., 94 % helium and 6 % nitrogen) for the injector stage and a variable-length gas cell filled with pure helium for the accelerator stage. Designing parameters of the laser wakefield accelerator can be carried out by relying on the scaling law of nonlinear plasma wakefields in the bubble regime [31–33]. Provided that a laser pulse with 41 TW peak power and 85 fs duration is focused on 12 μm spot radius on the entrance of the injector cell operated at plasma density of $3.3 \times 10^{18} \text{ cm}^{-3}$, strong nonlinear wakefields can be generated so that a 1.6 nC electron bunch could be trapped due to ionization-induced injection [34, 35] and accelerated up to 40 MeV, followed by boosting its energy up to 210 MeV at the length of 2.6 cm in the accelerator cell operated at plasma density of $1.1 \times 10^{18} \text{ cm}^{-3}$. The relative energy spread and the normalized emittance of resultant output beams are estimated to be 4 % in r.m.s.

and 0.15 mm mrad, respectively.

The electron bunch is then focused via a set of permanent-magnet-based quadrupoles (PMQs) [36] consisting of three elements -275 T/m, 770 T/m and -650 T/m with the common inner radius 3.0 mm and outer radius 12.0 mm, respectively, over 71.2 cm as shown in Fig.5 which displays variations of the horizontal and vertical beam envelopes simulated by TRACE3D [37] for the given incident parameters of the LPA configuration above.

Based on these counter-propagating electron beams, we evaluate the number of incident γ -rays produced by the inverse nonlinear Compton process between a circularly polarized laser pulse and an unpolarized electron bunch produced by LPA. It is worth noting that once we fix the focusing geometry, we cannot increase the effective number of γ -rays as much as we like even if we could increase the laser pulse energy. This is because of the nonlinear nature of Compton scattering represented by the parameter $\eta \equiv e\sqrt{-\langle A_\mu A^\mu \rangle}/mc^2$ where A_μ is the four-vector potential of the laser pulse [38]. The η parameter increases the effective electron mass $m^* = m\sqrt{1 + \eta^2}$ in the laser field. Hence, the scattered photon energy in the single photon absorption case is effectively lowered and the photon yield in the Compton edge energy also diminishes. On the other hand, the larger number of laser photons increases the luminosity factor in the Compton scattering. Therefore, there is an optimal η value so that the scattered photon energy is kept within 0.5-1.0 MeV range with the maximized γ -ray yield.

In Fig.6, we plot this situation in three different η cases: solid ($\eta = 0.31$), dashed ($\eta = 0.63$) and dash-dotted ($\eta = 0.88$). Figure 6 a) shows the differential cross sections $d\sigma_{el}^{(\pm)}/d\theta$ in units of $(\mu\text{m})^2/\text{rad}$ as a function of photon scattering angle measured from the incident direction of the electron beam, where the abscissa is displayed in units of $1/\gamma^*$ with the Lorentz factor defined by the effective electron mass in the laser field. The symbols (\pm) denote circular polarization flip $(-)$ and non-flip $(+)$ cases in the transition between the initial and final state photons. The $(-)$ and $(+)$ cases are plotted with thicker and thinner lines, respectively. The cross sections are numerically calculated based on the expressions available in Ref. [38]. In any η cases, in order to enhance the purity of the $(-)$ case, we must consider γ -rays produced only in $\theta < 1/\gamma^*$ as the effective number of γ -rays useful for the test of helicity specified $\gamma\gamma$ -scatterings. Figure 6 b) shows E_{cms} distributions by taking all possible energy combinations between two incident γ -rays from the Compton scattering points with the cross section weights in the $(-)$ case within $\theta < 1/\gamma^*$ in Fig.6 a),

where the area of the distributions indicate squares of the numbers of generated γ -rays, N_γ , corresponding to the numerators in the luminosity factor for the $\gamma\gamma$ -collider as we discuss below.

The head-on luminosity factor for $\gamma\gamma$ -scattering is defined as $\frac{fN_\gamma^2}{4\pi r_b^2}$ where we assume $\gamma\gamma$ -collisions take place along the electron beam axis within the effective γ -beam radius at IP, r_b . Because the distance between the two CP points, D , should be kept as small as possible to increase N_γ , r_b effectively coincides with the beam waist of the Compton seed laser, w_0 , if the electron beam radius is much smaller than w_0 . On the other hand, in order to enrich the $+$ \rightarrow *any* case in the QED-based $\gamma\gamma$ -scattering, the requirement to enhance the $(-)$ case by limiting the effective scattering angle $\theta < 1/\gamma^*$ demands the relation $D/\gamma^* = w_0$. This implies that we can control the purity of the initial circular polarization states by adjusting D in experiments.

IV. DESIGN OF THE DETECTION SYSTEM

We summarize optimal parameters for an all-optical photon-photon collider in the case of $\eta = 0.63$ in Table 1. For instance, if we apply this detection system to two synchronized lasers operated at $f \sim 10$ Hz, a data taking period over several months will be sufficient to claim the statistical significance of the QED-based elastic scattering events for the $+$ \rightarrow *any* case.

Due to the short D , we simultaneously have to consider electron-electron scattering after the inverse Compton scattering occurs, because this Møller's scattering can produce dominant background events against the elastic $\gamma\gamma$ -scattering as shown in Fig.7 a) and b). However, as far as only large angle scattering events in the range of $\vartheta = 45 - 135$ degree are measured, the partially integrated cross section of Møller's scattering over that solid angle is suppressed to $17.7 \mu\text{b}$ for the electron energy of 210 MeV, which is evaluated by the following differential cross section with respect to solid angle $\frac{d\sigma_M}{d\Omega} = \frac{\alpha^2}{4E^2(E^2-m^2)^2} \left[\frac{4(2E^2-m^2)^2}{\sin^4\vartheta} - \frac{8E^4-4E^2m^2-m^4}{\sin^2\vartheta} + (E^2-m^2)^2 \right]$ where E is the incident electron energy in the center-of-mass system. On the other hand, the cross section of QED $\gamma\gamma$ -scattering is relatively enhanced over the background events in the same ϑ range. Taking the higher luminosity factor for the electron-electron scattering than that of $\gamma\gamma$ -scattering into account, the event rate for Møller's scattering reaches 0.36 Hz for $f = 10$ Hz and the accidental rate

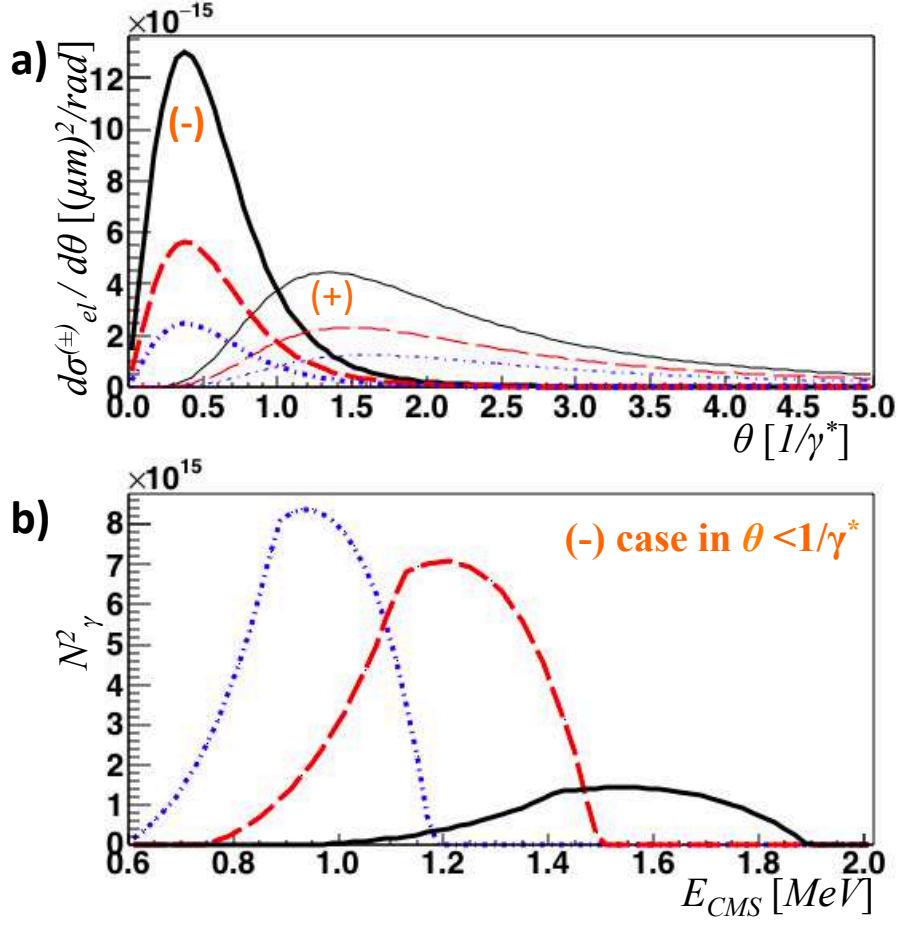


FIG. 6: Nonlinear effects in Compton scattering with $\eta = 0.31$ (solid), 0.63 (dashed) and 0.88 (dash-dotted) : a) differential Compton scattering cross sections $\sigma_{el}^{(\pm)}/d\theta$ as a function of photon scattering angle measured from the incident direction of the electron beam in units of $1/\gamma^*$ with the Lorentz factor of the effective electron mass in the laser field. The symbols (\pm) denote circular polarization flip $(-)$ and non-flip $(+)$ cases in the transition between the initial and final state photons. b) E_{cms} distributions by taking all possible energy combinations between two incident γ -rays from the Compton scattering points with the cross section weights in the case of $(-)$ in $\theta < 1/\gamma^*$, where the distributions are normalized to squares of the numbers of generated γ -rays.

for two types of scattering events to occur within the same shot can be evaluated as 2.6×10^{-6} Hz. This contaminated event rate corresponds to 36 % of that of the QED $\gamma\gamma$ -scattering. Therefore, even if one throws such contaminated events away without the detailed event-by-event offline analysis, the statistical loss of the QED events is still acceptable. In reality, the energy deposits on the detector as well as the event topologies, whether electromagnetic

TABLE I: Parameters for the all-optical photon-photon collider LPA drive laser

LPA drive laser	
Wavelength [μm]	0.8
Repetition rate [Hz]	10
Pulse energy [J]	3.5
Peak power [TW]	41
Pulse duration [fs]	85
LPA electron beam	
Beam energy [MeV]	210
Plasma density [10^{18} cm^{-3}]	1.1
Accelerator length [cm]	2.6
Charge per bunch [nC]	1.6
Bunch duration [fs]	~ 10
Normalized emittance [mm mrad]	~ 0.15
Horizontal rms beam size at Compton IP [μm]	0.8
Vertical rms beam size at Compton IP [μm]	0.5
Laser for Compton scattering	
Wavelength [μm]	0.8
Repetition rate [Hz]	10
Pulse energy [mJ]	89
Pulse duration [fs]	209
Spot radius at Compton IP [μm]	4.0
Interaction angle [degree]	0
Focused intensity [10^{17} W/cm^2]	8.5
Compton γ -ray beam	
Photon energy between $\theta = 0 - 1/\gamma^*$ rad [MeV]	0.37-0.75
Effective photon flux [10^9 s^{-1}]	8.65
Effective spot radius r_b at $\gamma\gamma$ -IP [μm]	4.0
$\gamma\gamma$ -scattering	
Averaged CMS photon-photon collision energy [MeV]	1.5
Averaged QED cross section [μb]	3.33
Rate of QED events [10^{-6} s^{-1}]	2.4

showers exist or not, are very different between QED $\gamma\gamma$ -scattering and Møller's scattering as displayed in Fig.7 a) and b). Therefore, one can readily distinguish two types of scattering events at the offline analysis and possibly distinguish them even within the same shot, if the two γ -clusters are sufficiently isolated from the background electromagnetic showers. Moreover, counting the number of Møller's scattering events is indispensable to directly measure the electron-electron luminosity in the actual experimental condition. This information is essentially important to deduce the $\gamma\gamma$ luminosity in addition to the direct measurement of the γ -ray flux.

V. CONCLUSION

Verification of the QED-based helicity dependent light-by-light scattering with the all-optical photon-photon collider is realizable in the table-top scale. Provided PW-class lasers such as Extreme Light Infrastructure (ELI) [39] we may be able to test the QED-based light-by-light scattering especially in the same circular polarization case of incident γ -rays with an experimentally feasible rate. Furthermore, the rapid development of fiber-based high-power and high-repetition rate lasers at 10 kHz [40] would allow us to test the opposite circular polarization case and enable the comparison between the two helicity configurations quantitatively. The larger statistics also opens up opportunities to perform general resonance searches around the MeV energy scale based on the landmark of quantitative verification of the QED-based perturbative photon-photon scattering. Finally we emphasize that our proposal corresponds to the first case of LPA-based electron-electron and $\gamma\gamma$ -colliders applied to fundamental particle physics. If succeeded, it would be a ground-breaking advancement in experimental particle physics even if the center of mass energy is still in the MeV range.

Acknowledgments

We cordially thank Y. Iwashita for deeply considering the possibility to introduce the permanent-magnet-based dipole at IP in the electron transport line to avoid Møller's scattering in advance. K. Homma appreciates E. Milotti and C. Curceanu for discussions on the derivation for the QED-based cross section. He also acknowledges for the support by the Collaborative Research Program of the Institute for Chemical Research, Kyoto University

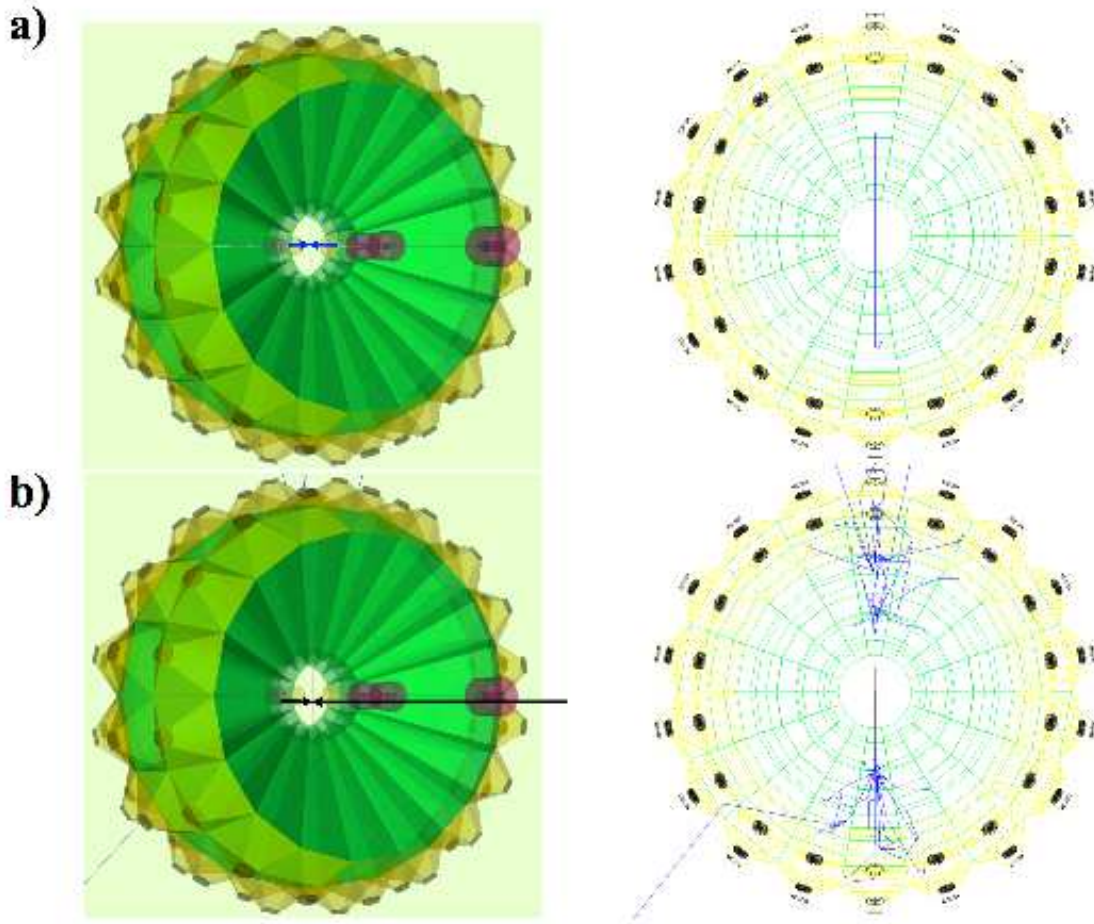


FIG. 7: Comparison of event displays simulated by GEANT4 for a) a QED-based $\gamma\gamma \rightarrow \gamma\gamma$ event and b) a background $e^-e^- \rightarrow e^-e^-$ event, where the blue and black trajectories denote photons and electrons, respectively. The detector system covers the polar angle $\vartheta = 45 - 135$ degree and the azimuthal angle $\varphi = 0 - 360$ degree around the beam axis consisting of 90 scintillator crystals (18 crystals in $\varphi \times 5$ layers in ϑ) made of Ce doped Gd_2SO_5 (GSO:Ce). GSO:Ce is a well-balanced scintillator from the point of view on the scintillation-photon yield for a sub-MeV γ -ray, the time resolution and the radiation length X_0 . The radiation length $X_0 = 1.38$ cm is reasonably small to suppress the lateral spreads of the electromagnetic showers produced by 210 MeV electrons. The individual crystal has the depth of $10X_0$.

(grants No. 2015-93). K. Nakajima was supported by the Project Code (IBS-R012-D1).

- [1] Akhmadaliev, Sh. Zh. et al., Phys. Rev. C58 2844-2850 (1998).
- [2] Meitner, L. and Kösters, H., Z. Phys. 84, 137 (1933).
- [3] d'Enterria, D. and da Silveira, G. G., Phys. Rev. Lett. 111, 080405 (2013).
- [4] Halpern, O., Phys. Rev. 44, 855 (1934).
- [5] Toll, J. S., *The Dispersion Relation for Light and its Application to Problems Involving Electron Pairs*, PhD thesis, Princeton, 1952 (unpublished).
- [6] Karplus, R. and Neuman, M., Phys. Rev. 83: 776-784 (1950).
- [7] De Tollis, B., Nuovo Cimento 32, 757 (1964).
- [8] De Tollis, B., Nuovo Cimento 35, 1182 (1965).
- [9] Inada, T. et al., Phys. Lett. B 732: 356-359 (2014).
- [10] Moulin, F., Bernard, D. and Amiranoff, F., Z. Phys. C 72 : 607-611 (1996).
- [11] Bernard, D. et al., Eur. Phys. J. D 10 : 141-145 (2000).
- [12] Homma, K., Hasebe, T., and Kume, K., Prog. Theor. Exp. Phys. 083C01 (2014).
- [13] Fouche, M., BMV Collaboration, et al., iPhys. Rev. D 78 , 032013 (2008).
- [14] Robilliard, C., BMV Collaboration, et al., Phys. Rev. Lett. 99, 190403 (2007).
- [15] Cameron, R., BRFT Collaboration, et al., Phys. Rev. D 47, 3707 (1993).
- [16] Chou, A. S., GammeV (T-969) Collaboration, et al., Phys. Rev. Lett., 100, 080402 (2008).
- [17] Afanasev, A. LIPSS Collaboration, et al., Phys. Rev. Lett. 101, 120401 (2008).
- [18] Pugnati, P., OSQAR Collaboration, et al., Phys. Rev. D 78, 092003 (2008).
- [19] Zavattini, E., PVLAS Collaboration, et al., Phys. Rev. D 77 , 032006 (2008).
- [20] Ehret, K., ALPS Collaboration, et al., Phys. Lett. B 689: 149-155 (2014).
- [21] Bregant, M. et al., Phys. Rev. D 78, 032006 (2008).
- [22] Lundstrom, E., Brodin, G., Lundin, J., Marklund, M., Bingham, R., Collier, J., Mendonca, J. T. and Norreys, P., Phys. Rev. Lett. 96, 083602 (2006)
- [23] Heinzl, T., Liesfeld, B., Amthor, K. -U, Schwoerer, H., Sauerbrey, R. and Wipf, A., Opt. Commun. **267**, 318 (2006)
- [24] King, B., Di Piazza, A. and Keitel, C.H., Nature Photonics 4, 92-94 (2010).
- [25] Homma, K., Habs, D. and Tajima, T., Applied Physics B Laser and Optics 104:769-782 (2011).

- [26] Euler, H. and Kockel, B., *Naturwiss.* 23, 246 (1935).
- [27] Heisenberg, W. and Euler, H., *Z. Phys.* 98, 714 (1936).
- [28] Dinu, V., Heinzl, T., Ilderton, A., Marklund, M. and Torgrimsson, G., *Phys. Rev. D* 89, 125003 (2014).
- [29] Dinu, V., Heinzl, T., Ilderton, A., Marklund, M. and Torgrimsson, G., *Phys. Rev. D* 90, 045025 (2014).
- [30] Tajima, T. and Dawson, J. M., *Phys. Rev. Lett.* 43, 267 (1979).
- [31] Kostyukov, I. et al., *Phys. Plasmas* 11, 5256 (2004).
- [32] Lu, W. et al., *Phys. Rev. ST Accel. Beams* 10, 061301 (2007).
- [33] Nakajima, K., *High Power Laser Science and Engineering* 2, e31, (2014).
- [34] Pak, A. et al., *Phys. Rev. Lett.* 104, 025003 (2010).
- [35] Chen, M. et al., *Phys. Plasmas* 19, 033101 (2012).
- [36] Halbach, K., *Nucl. Instr. Meth.* 169:110.
- [37] Crandall, K. and Rusthoi, D., Los Alamos National Laboratory Technical Report No. LA-UR-97-886, 1997.
- [38] Shmakov, K. D., *Study of nonlinear QED effects in interactions of terawatt laser with high-energy electron beam*, SLAC-R-666, UMI-98-23127, UMI-98-23127-MC.
- [39] <http://www.eli-np.ro>; <http://www.eli-beams.eu>; <http://www.eli-alps.hu>.
- [40] Mourou, G., Brocklesby, B., Tajima, T., Limpert, J., *Nature Photonics* 7, 258261 (2013).